

# UAV Formation Preservation for Target Tracking Applications

Aditya Hegde<sup>1,\*</sup>, Jasmine Jerry Aloor<sup>2,\*</sup> and Debasish Ghose<sup>1</sup>

**Abstract**—This paper presents a collaborative target tracking application with multiple agents and a formulation of an agent-formation problem with desired inter-agent distances and specified bounds. We propose a barrier Lyapunov function-based distributed control law to preserve the formation for target-tracking and assess its stability using a kinematic model. Numerical results with this model are presented to demonstrate the advantages of the proposed control over a quadratic Lyapunov function-based control. A concluding evaluation using experimental ROS simulations is presented to illustrate the applicability of the proposed control approach to a multi-rotor system and a target executing straight line and circular motion.

## I. INTRODUCTION

Uncrewed Aerial Vehicles (UAVs) are widely used in area exploration [1], agriculture [2], payload transportation [3], and target tracking [4] applications. Recently, UAV-based target-tracking applications have received significant attention and relevant work has been done to visually track moving objects [5]. The object tracking problem is extended to cases with multiple moving objects, and the visual identification and tracking of UAVs have been performed by a camera mounted on another UAV [6]. Collaborative object tracking, as discussed in [7] involves a team of UAVs tracking the object one at a time, depending on battery charge. Unlike the application discussed in [7], we consider a simultaneous object tracking problem involving a team of UAVs that hold their formation as they accomplish the target-tracking task. Using multiple UAVs provides robustness to the object tracking problem.

Applying multi-agent system theory to construct and operate UAV formations adds several benefits over operating individual UAVs by adding redundancy [8], augmenting information availability [9], and reducing task completion time. The added complexity, however, (1) adversely affects system stability and performance characterisation and (2) imposes additional constraints limiting complete utilisation of the benefits of operating formations.

An imposition of agent interaction radius may lead to a time-varying interaction topology for the system [10], which adds stochasticity to the prediction of system state evolution and stability analysis. Interaction and connectivity maintenance are thus essential for collaborative tasks, and control needs to be applied to the agents to preserve

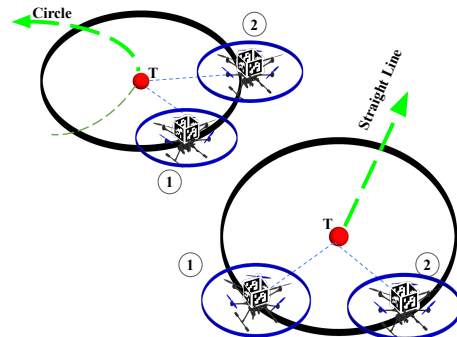


Fig. 1. Summary of the approach: Two hexarotors track a continuously moving target while maintaining a distinct formation (their mutual separation)

the connectivity of the network [11]. In formations, these constraints are placed on inter-agent distances so that each agent can preserve its interaction with its neighbours [12]. Extensive work has been done in the area of multi-objective multi-agent systems, with collision avoidance included as a constraint in the formulation of Lyapunov-like barrier functions [13]. Formation control and preservation in the presence of communication and measurement uncertainties are discussed in [14]. In line with the formation preservation requirements of a collaborative target tracking application, we build on the idea of graph rigidity theory of formation control [15], by specifying bounds on inter-agent distances. In doing so,

- 1) the formulation allows minimal deviation of the inter-agent distances from the reference distances in a rigid formation, thus accounting for decentralised control applications which suffer from limited communication bandwidth and processing power, requiring operating bounds instead of a set point.
- 2) the formulation also constrains agent-relative motion, thus maintaining the topology of the formation.

We enforce the aforementioned bounds using barrier Lyapunov functions [16], [17] (BLFs) and construct Lyapunov-like functions for a multi-objective problem using decentralised control. Collaborative target-tracking applications may require the UAVs to track targets farther away, and the Lyapunov function-based multi-objective formulations, as presented in this paper, require one or a few objectives (formation preservation) to be given a higher priority. Thus, existing approaches to Lyapunov function-based formation control [18] do not apply to problems with such requirements. Further, existing literature [19] relies on assigning leader-follower roles to the agents in a formation, thus

<sup>1</sup>Aditya Hegde and Debasish Ghose are with the Department of Aerospace Engineering, Indian Institute of Science, Bangalore adityahegde@iisc.ac.in, dghose@iisc.ac.in

<sup>2</sup>Jasmine Jerry Aloor is with the Department of Aerospace Engineering, Indian Institute of Technology, Kharagpur jasminejerry@iitkgp.ac.in

\*Authors contributed equally to this work

avoiding multi-objective control formulations for the agents. In contrast to this, we assume homogeneous roles for the agents in our work and present a multi-objective constrained control algorithm for each agent in the formation. Results with a kinematic model of agents, as well as with hexa-rotor models in the ROS environment, are presented to demonstrate the practical applicability of the proposed formulation and associated control.

The organisation of the paper is as follows - Section II discusses the preliminaries and the system model. We cover the objectives of the target tracking problem, propose the control, assess its stability and provide numerical results with a kinematic model in Section III. Section IV presents ROS simulation results and practical applicability of the proposed approach. The paper is concluded with a discussion on the planned future work in Section V.

## II. SYSTEM DESCRIPTION AND OTHER PRELIMINARIES

This section introduces the system model, notations and definitions required for subsequent analysis.

### A. Preliminaries

The sets of real and non-negative real numbers are represented by  $\mathbb{R}$  and  $\mathbb{R}_+$ , respectively. Vectors are represented by lowercase boldface and matrices by uppercase boldface notations. A differentiable function  $f: \mathcal{D} \rightarrow \mathbb{R}$ ,  $\mathcal{D} \subseteq \mathbb{R}^n$  has a gradient  $\nabla_{\mathbf{x}} f = \left[ \frac{\partial f}{\partial x_1}, \frac{\partial f}{\partial x_2}, \dots, \frac{\partial f}{\partial x_n} \right]^T$ ,  $\forall \mathbf{x} = [x_1, x_2, \dots, x_n]^T \in \mathcal{D}$ . We use the  $L_2$ -norm in the subsequent sections and represent it by  $\|\cdot\|$ . We represent the inner product of  $\mathbf{x}_1, \mathbf{x}_2 \in \mathbb{R}^n$  as  $\mathbf{x}_1 \cdot \mathbf{x}_2$ . The Cartesian product  $\mathbb{R}^2 \times \mathbb{R}^2, \dots \times \mathbb{R}^2$  ( $N$ -times) is represented by  $\mathbb{R}^{2N}$ , where  $\times$  represents the Cartesian product operator. We represent the formation of agents with an undirected graph  $\mathcal{G} = (\mathcal{V}, \mathcal{E})$ , where the agents represent the elements of the finite set  $\mathcal{V}$  and their interactions are represented as an unordered pair  $(i, j) \in \mathcal{E} \subseteq \mathcal{V} \times \mathcal{V}$ ,  $i, j \in \mathcal{V}$ .

### B. System Model

We consider a system of  $N$  agents moving in the  $\mathbb{R}^2$  plane. The agents are holonomic, have first-order dynamics, and are represented by

$$\dot{\mathbf{x}}_k = \mathbf{v}_k = \mathbf{u}_k, \quad k \in \{1, 2, \dots, N\} \quad (1)$$

where,  $\mathbf{x}_k$ ,  $\mathbf{v}_k$ , and  $\mathbf{u}_k$  are the position, velocity and control input for the  $k^{\text{th}}$  agent. The control input  $\mathbf{u}_k$  in (1) is further considered to be constrained as below

$$\mathbf{u}_k = \text{sat}(\|\mathbf{u}_k\|, u_{\max}) \hat{\mathbf{u}}_k := \begin{cases} \mathbf{u}_k & \text{if } \|\mathbf{u}_k\| \leq u_{\max} \\ u_{\max} \hat{\mathbf{u}}_k, & \text{if } \|\mathbf{u}_k\| > u_{\max} \end{cases} \quad (2)$$

where,  $\hat{\mathbf{u}}_k$  is the unit vector along the direction of  $\mathbf{u}_k$ .

This system of agents is a simple representation for a system of multi-rotors executing planar motion, with constraints placed on their velocity inputs, motivated by the PX4 autopilot [20] used for velocity-based control of multi-rotors (simulated in the Robot Operating System (ROS) environment and discussed in Section IV). The model is beneficial for a preliminary stability analysis of the formation

preservation algorithm presented here. Such a team of multi-rotors may be required to survey an area, track a target [21], or deliver a payload [22].

*Remark 1:* The system model (1) is chosen to align with the PX4 implementation of velocity reference-based PID control (used in the ROS simulations) and the BLF-based distance-bounding control proposed in this paper is extendable to systems modelled using second-order dynamics.

### C. Barrier Lyapunov function

Barrier Lyapunov functions (BLFs) provide the framework for ensuring constrained system operation [16]. They extend the idea of control Lyapunov functions (CLFs) by inherently including the constraints in the function and associated control law formulation. They have been extended to multi-objective multi-agent problems requiring one or a few objectives to be performance-bounded [23].

*Definition 1 (Barrier Lyapunov Function [16]):* A Barrier Lyapunov Function is a scalar function  $V(\mathbf{x})$  of state vector  $\mathbf{x} \in \mathcal{D}$  of the system  $\dot{\mathbf{x}} = f(\mathbf{x})$  on an open region  $\mathcal{D}$  containing the origin, that is continuous, positive definite, has continuous first-order partial derivatives at every point of  $\mathcal{D}$ , has the property  $V(\mathbf{x}) \rightarrow \infty$  as  $\mathbf{x}$  approaches the boundary of  $\mathcal{D}$ , and satisfies  $V(\mathbf{x}(t)) \leq b, \forall t \geq 0$ , along the solution of  $\dot{\mathbf{x}} = f(\mathbf{x})$  for  $\mathbf{x}(0) \in \mathcal{D}$  and some positive constant  $b$ .

*Lemma 1 ([16]):* For any positive constants  $k_{a_1}, k_{b_1}$ , let  $\mathcal{Z} := \{z \in \mathbb{R} \mid -k_{a_1} < z < k_{b_1}\} \subset \mathbb{R}$  and  $\mathcal{N} := \mathbb{R}^\ell \times \mathcal{Z} \subset \mathbb{R}^{\ell+1}$  be open sets. Consider the system  $\dot{\boldsymbol{\eta}} = \mathbf{h}(t, \boldsymbol{\eta})$ , where,  $\boldsymbol{\eta} := [\mathbf{w}, z]^T \in \mathcal{N}$ , and  $\mathbf{h}: \mathbb{R}_+ \times \mathcal{N} \rightarrow \mathbb{R}^{\ell+1}$  is piecewise continuous in  $t$  and locally Lipschitz in  $\boldsymbol{\eta}$ , uniformly in  $t$ , on  $\mathbb{R}_+ \times \mathcal{N}$ . Suppose that there exist functions  $U: \mathbb{R}^\ell \rightarrow \mathbb{R}_+$  and  $V_1: \mathcal{Z} \rightarrow \mathbb{R}_+$ , continuously differentiable and positive definite in their respective domains, such that  $V_1(z) \rightarrow \infty$  as  $z \rightarrow -k_{a_1}$  or  $z \rightarrow k_{b_1}$ , and  $\gamma_1(\|\mathbf{w}\|) \leq U(\mathbf{w}) \leq \gamma_2(\|\mathbf{w}\|)$ , where,  $\gamma_1$  and  $\gamma_2$  are class  $\mathcal{K}_\infty$  functions. Let  $V(\boldsymbol{\eta}) := V_1(z) + U(\mathbf{w})$ , and  $z(0) \in \mathcal{Z}$ . If  $\dot{V} = (\nabla_{\boldsymbol{\eta}} V) \cdot \mathbf{h} \leq 0$  holds, then  $z(t) \in \mathcal{Z}, \forall t \in [0, \infty)$ .

In the next section, we will use Lemma 1 to construct a multi-objective Lyapunov-like function for each agent subjected to constraints.

## III. COLLABORATIVE TARGET TRACKING AND FORMATION PRESERVATION

The collaborative target tracking problem involves two aspects - target tracking by the individual agents and formation preservation. Formation preservation is necessary to maintain communication between the agents for sharing and collecting target information. In this section, we identify these aspects as independent objectives and construct Lyapunov-like barrier functions. We then construct a multi-objective Lyapunov-like function and propose feedback control algorithms for the individual agents with given information availability and control architecture.

The positions of the target and the  $k^{\text{th}}$  agent in the inertial frame are  $\mathbf{x}_T \in \mathbb{R}^2$  and  $\mathbf{x}_k \in \mathbb{R}^2$ , respectively. It is assumed that the target velocity,  $\dot{\mathbf{x}}_T = \mathbf{v}_T$  is known. Each agent (for  $k \in \{1, 2, \dots, N\}$ ) tracks the target, while maintaining its interaction with other agents (see Fig. 2).

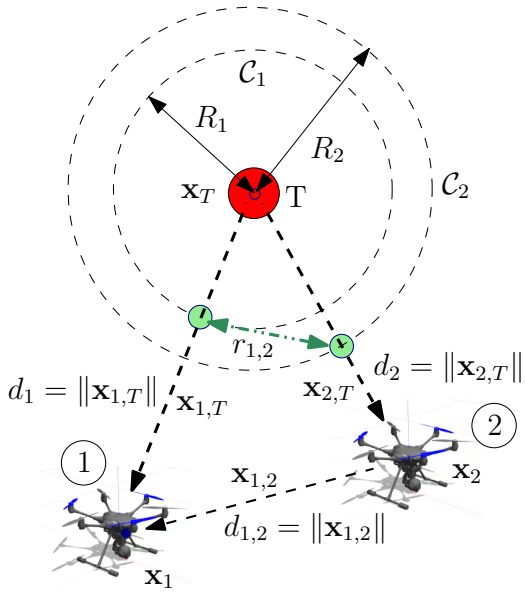


Fig. 2. Target tracking by two agents, with relevant inter-agent/target distances and desired configuration

### A. Target Tracking

The distance of the  $k^{\text{th}}$  agent from the target is  $d_k = \|\mathbf{x}_k - \mathbf{x}_T\| = \|\mathbf{x}_{k,T}\|$ , and it is required to settle on a standoff circle  $\mathcal{C}_k$  about the target, with a radius  $R_k$ . A two agent target-tracking problem is shown in Fig. 2 with agents settling on separate standoff circles. Such a case may arise when one of the agents may be required to be closer to the target than the other, due to sensor limitations. A Lyapunov function,  $U(\mathbf{x})$ , is proposed for system (1),

$$U(\mathbf{x}, \mathbf{x}_T) = \sum_{k=1}^N U_k(\mathbf{x}_k, \mathbf{x}_T) = \frac{1}{4} \sum_{k=1}^N (d_k^2 - R_k^2)^2 \quad (3)$$

where,  $U_k(\mathbf{x}, \mathbf{x}_T) = \frac{1}{4}(d_k^2 - R_k^2)^2$  is the Lyapunov function for the  $k^{\text{th}}$  agent. The time derivative of  $U(\mathbf{x}, \mathbf{x}_T)$  is

$$\begin{aligned} \dot{U}(\mathbf{x}, \mathbf{x}_T) &= \sum_{k=1}^N \dot{U}_k(\mathbf{x}_k, \mathbf{x}_T) = \sum_{k=1}^N \nabla_{\mathbf{x}_{k,T}} U_k \cdot \dot{\mathbf{x}}_{k,T} \\ &= \sum_{k=1}^N d_k (d_k^2 - R_k^2) \hat{\mathbf{x}}_{k,T} \cdot \dot{\mathbf{x}}_{k,T} \end{aligned} \quad (4)$$

where,  $\hat{\mathbf{x}}_{k,T}$  is the unit vector along the line joining the target to the agent, and the relation  $\nabla_{\mathbf{x}_{k,T}} U_k = d_k (d_k^2 - R_k^2) \hat{\mathbf{x}}_{k,T}$  is used to simplify the expression.

### B. Formation Preservation and Collaborative Tracking

The formation preservation problem requires the maintenance of inter-agent distances in the formation. However, the use of decentralised and distributed control in practical applications makes the maintenance of formation rigidity difficult, requiring the placement of bounds (symmetric or asymmetric) on inter-agent distances. These bounds are included as constraints in the BLF associated with each pair of agents  $(i, j) \in \mathcal{E}$ . The BLF for the system associated with

formation preservation is

$$\begin{aligned} V(\mathbf{x}) &= \sum_{(i,j) \in \mathcal{E}} V_{i,j}(\mathbf{x}_i, \mathbf{x}_j) \\ &= \frac{1}{2} \sum_{(i,j) \in \mathcal{E}} \frac{(d_{i,j}^2 - r_{i,j}^2)^2}{(\bar{r}_{i,j}^2 - d_{i,j}^2)(d_{i,j}^2 - \underline{r}_{i,j}^2)} \end{aligned} \quad (5)$$

where,  $d_{i,j} = \|\mathbf{x}_i - \mathbf{x}_j\| = \|\mathbf{x}_{i,j}\|$  and  $r_{i,j}$  is the desired inter-agent distance between each pair of interacting agents (see Fig. 2). The lower and upper bounds on the inter-agent distances for each pair are  $\underline{r}_{i,j}$  and  $\bar{r}_{i,j}$  (see Fig. 3). The time derivative of  $V(\mathbf{x})$  is

$$\begin{aligned} \dot{V}(\mathbf{x}) &= \sum_{(i,j) \in \mathcal{E}} \dot{V}_{i,j}(\mathbf{x}_i, \mathbf{x}_j) \\ &= \sum_{(i,j) \in \mathcal{E}} \nabla_{\mathbf{x}_{i,j}} V_{i,j} \cdot \dot{\mathbf{x}}_{i,j} \\ &= \sum_{(i,j) \in \mathcal{E}} \frac{ad_{i,j} (2b - a(\bar{r}_{i,j}^2 - 2d_{i,j}^2 + \underline{r}_{i,j}^2))}{b^2} \hat{\mathbf{x}}_{i,j} \cdot \dot{\mathbf{x}}_{i,j} \end{aligned} \quad (6)$$

where,  $a = d_{i,j}^2 - r_{i,j}^2$ ,  $b = (\bar{r}_{i,j}^2 - d_{i,j}^2)(d_{i,j}^2 - \underline{r}_{i,j}^2)$  and  $\nabla_{\mathbf{x}_{i,j}} d_{i,j} = \hat{\mathbf{x}}_{i,j}$  have been used to make the expression compact. The preservation of the interaction topology requires both agents in a pair  $(i, j)$  to be active in maintaining the inter-agent distance within bounds. We now propose a control law using Lemma 1, with the functions  $U(\mathbf{x})$  and  $V(\mathbf{x})$  representing the target-tracking and formation preservation objectives of the problem.

*Theorem 1:* Let  $\mathcal{G} = (\mathcal{V}, \mathcal{E})$  be the undirected and connected graph representing a formation of  $N$  agents. Consider agent model (1), with initial states of the agents in the set  $\mathcal{X}_r := \{(\mathbf{x}_1, \mathbf{x}_2, \dots, \mathbf{x}_N) \in \mathbb{R}^{2N} \mid \underline{r}_{i,j} < d_{i,j} < \bar{r}_{i,j}, \forall (i, j) \in \mathcal{E}\}$ , where  $d_{i,j}$  is defined in (5), and  $\underline{r}_{i,j}, \bar{r}_{i,j} > 0$  are positive constants for  $(i, j) \in \mathcal{E}$ . Assuming that the target velocity  $\mathbf{v}_T$  is known, let the following saturated control law (2) be applied to the agents

$$\begin{aligned} \mathbf{u}_k &= \mathbf{v}_T - K_T d_k (d_k^2 - R_k^2) \hat{\mathbf{x}}_{k,T} \\ &\quad - K \sum_{j|(k,j) \in \mathcal{E}} \frac{ad_{k,j}}{b^2} \{2b - a(\bar{r}_{k,j}^2 - 2d_{k,j}^2 + \underline{r}_{k,j}^2)\} \hat{\mathbf{x}}_{k,j} \end{aligned} \quad (7)$$

where,  $a$  and  $b$  are as defined in (6), and  $\|\mathbf{v}_T\| < u_{\max}$  for all  $k \in \{1, 2, \dots, N\}$ . Then, the following statements hold:

- i) If  $K_T, K > 0$ , all the agents asymptotically converge to the formation defined by  $\underline{r}_{i,j} \leq r_{i,j} \leq \bar{r}_{i,j}, \forall (i, j) \in \mathcal{E}$ .
- ii) The trajectories of the agents stay within  $\mathcal{X}_r$  for  $t \geq 0$ , that is, the set  $\mathcal{X}_r$  is invariant for  $t \geq 0$ .

*Proof:* To prove the two statements together, we construct a combined Lyapunov-like function  $W(\mathbf{x}) = K_T U(\mathbf{x}, \mathbf{x}_T) + K V(\mathbf{x})$  for the system. The derivative of  $W(\mathbf{x})$

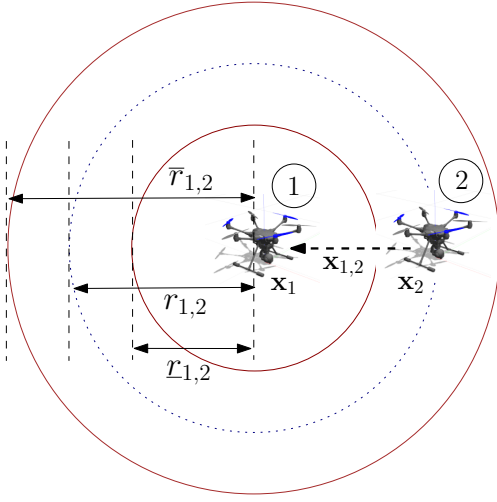


Fig. 3. A two-agent formation with desired inter-agent distance ( $r_{1,2}$ ), and associated lower ( $l_{1,2}$ ) and upper ( $\bar{r}_{1,2}$ ) bounds

is

$$\begin{aligned}
 \dot{W} &= K_T \sum_{k=1}^N \nabla_{\mathbf{x}_{k,T}} U_k \cdot \dot{\mathbf{x}}_{k,T} + K \sum_{(i,j) \in \mathcal{E}} \nabla_{\mathbf{x}_{i,j}} V_{i,j} \cdot \dot{\mathbf{x}}_{i,j} \\
 &= \sum_{k=1}^N \left( K_T \nabla_{\mathbf{x}_{k,T}} U_k + K \sum_{j|(k,j) \in \mathcal{E}} \nabla_{\mathbf{x}_{k,j}} V_{k,j} \right) \cdot \dot{\mathbf{x}}_{k,T} \\
 &= \sum_{k=1}^N \left( K_T \nabla_{\mathbf{x}_{k,T}} U_k + K \sum_{j|(k,j) \in \mathcal{E}} \nabla_{\mathbf{x}_{k,j}} V_{k,j} \right) \cdot (\mathbf{u}_k - \mathbf{v}_T)
 \end{aligned} \quad (8)$$

where, we use the relations  $\dot{\mathbf{x}}_{i,j} = \dot{\mathbf{x}}_{i,T} - \dot{\mathbf{x}}_{j,T}$  and  $\dot{\mathbf{x}}_{k,T} = \mathbf{u}_k - \mathbf{v}_T$  to simplify the expression. Using (7), and substituting the expressions for  $\nabla_{\mathbf{x}_{k,T}} U_k$  and  $\nabla_{\mathbf{x}_{k,j}} V_{k,j}$  from (4) and (6) we get  $\dot{W} = -\sum_{k=1}^N \|\mathbf{u}_k - \mathbf{v}_T\|^2 \leq 0$  along the closed loop solutions of system (1), when  $\|\mathbf{v}_T\| < u_{\max}$ .

The function  $W(t) = K_T U(t) + K V(t)$  is finite and bounded by  $W(t) \leq W(0) = K_T U(0) + K V(0), t \geq 0$  for finite initial distances of agents from the target  $d_k(0), \forall k \in \{1, 2, \dots, N\}$  and initial positions of the agents in the set  $\mathcal{X}_r$ . Thus, the positions of agents remain in  $\mathcal{X}_r$  for  $t \geq 0$ , proving (ii).

To prove (i), we note that the formation defined by  $r_{i,j} \leq r_{i,j}, \forall (i,j) \in \mathcal{E}$  represents the set  $\mathcal{X}_r$ . Thus, the multiple equilibrium formations corresponding to  $\mathbf{u}_k = \mathbf{v}_T$  and  $\dot{W} = \dot{U} = \dot{V} = 0$  satisfy the specified distance bounds, for an initial formation that satisfies them. ■

The proposed control for the  $k^{\text{th}}$  agent thus requires distance and bearing information of the target ( $T$ ) and its interacting agents  $j$  such that  $(k,j) \in \mathcal{E}$ , along with information of the target velocity,  $\mathbf{v}_T$ .

### C. Numerical Simulation Results

We present simulation results with control (7) applied to  $N = 3$  agents using system model (1) and the *SciPy* library in *Python*. The agents are required to settle on standoff circles  $\mathcal{C}_1 = \mathcal{C}_2 = \mathcal{C}_3$  about the target, with equal radii  $R_1 =$

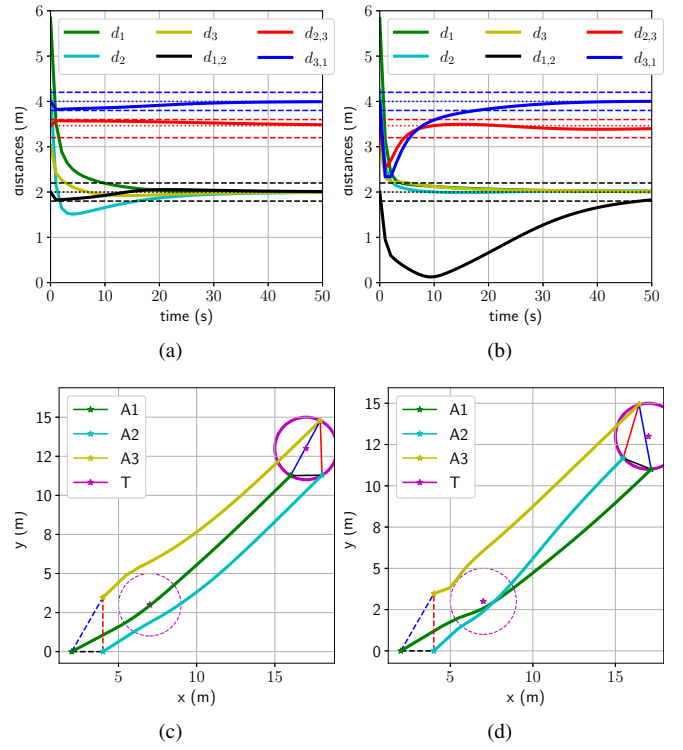


Fig. 4. A comparison of BLF and QLF-control for straight-line motion of target. Inter-agent and agent-target distances for (a) BLF-control and (b) QLF-control. Agent and target trajectories T - target; A1, A2, A3 - agents for (c) BLF-control (d) QLF-control

$R_2 = R_3 = 2$  m. The desired inter-agent distances and the associated bounds are listed below.

- 1)  $r_{1,2} = 2$  m,  $l_{1,2} = 1.8$  m,  $\bar{r}_{1,2} = 2.2$  m
- 2)  $r_{2,3} = 2\sqrt{3} \approx 3.46$  m,  $l_{2,3} = 3.2$  m,  $\bar{r}_{2,3} = 3.6$  m
- 3)  $r_{3,1} = 4$  m,  $l_{3,1} = 3.8$  m,  $\bar{r}_{3,1} = 4.2$  m

The gains in control (7) are  $K_T = 0.03$  and  $K = 0.01$ . The bound on the control input to agents is  $u_{\max} = 3$  m/s. We consider straight line and circular motion of the target and compare the results from using BLF control to a baseline scenario using quadratic Lyapunov function (QLF) of the form  $W_Q(\mathbf{x}) = K_T U(\mathbf{x}, \mathbf{x}_T) + K Q(\mathbf{x})$ . Here  $Q(\mathbf{x}) = \sum_{(i,j) \in \mathcal{E}} Q_{i,j}(\mathbf{x}_i, \mathbf{x}_j) = \frac{1}{4} \sum_{(i,j) \in \mathcal{E}} (d_{i,j}^2 - r_{i,j}^2)^2$  and the associated gradient-based QLF-control for the  $k^{\text{th}}$  agent is

$$\mathbf{u}_k = \mathbf{v}_T - K_T d_k (d_k^2 - R_k^2) \hat{\mathbf{x}}_{k,T} - K \sum_{j|(k,j) \in \mathcal{E}} d_{k,j} (d_{k,j}^2 - r_{k,j}^2) \hat{\mathbf{x}}_{k,j}. \quad (9)$$

Such a QLF-control does not include constraints on the inter-agent distances and allows for the formation to rearrange the cyclic order (topology) of its agents. Further, we consider the effect of noise in the target velocity, agent-target and inter-agent distance measurements used in the BLF and QLF-based control for the circular motion of the target.

1) *Straight-line motion of the target:* A moving target with velocity  $\mathbf{v}_T = [0.2, 0.2]^T$  m/s is considered. The initial inter-agent distances are at the desired values. The evolution of inter-agent distances and their associated bounds along with the agent-target distances are plotted in Fig. 4(a). A

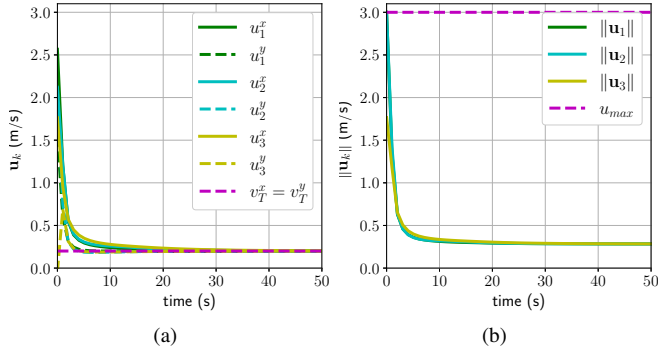


Fig. 5. Control inputs for straight-line motion of target. (a) BLF-control components tracking target velocity  $\mathbf{v}_T = [0.2, 0.2]$  m/s and (b) control magnitudes satisfying the bound  $u_{\max} = 3$  m/s

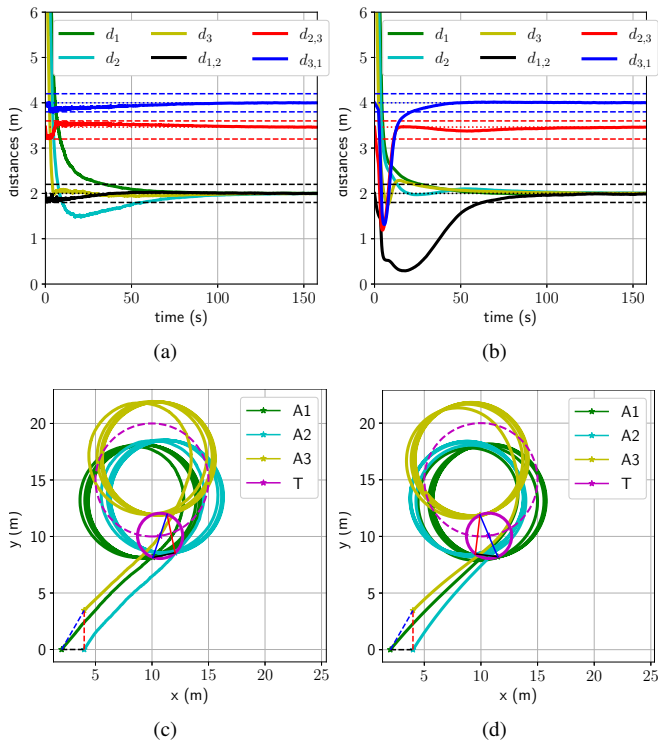


Fig. 6. A comparison of BLF and QLF-control for circular motion of target. Inter-agent and agent-target distances for (a) BLF-control and (b) QLF-control. Agent and target trajectories T - target; A1, A2, A3 - agents for (c) BLF-control (d) QLF-control

similar plot is presented for the QLF-control in Fig. 4(b). It is observed that the inter-agent distances using BLF-control (7) remain within the specified bounds (see  $d_{1,2}, d_{2,3}, d_{3,1}$  in Fig. 4(a)), while those in the case of QLF-control are unbounded (associated bounds are plotted in Fig. 4(b) for comparison with BLF-control). It is interesting to note the undershoot in the agent-target distances using BLF-control, which compensates for the bounded inter-agent distances, as compared to QLF-control.

The trajectories associated with the two control laws are plotted in Figs. 4(c) and 4(d). The initial and final positions of the triangular formation are plotted as dashed and solid lines. Similarly, the initial and final positions of the target and

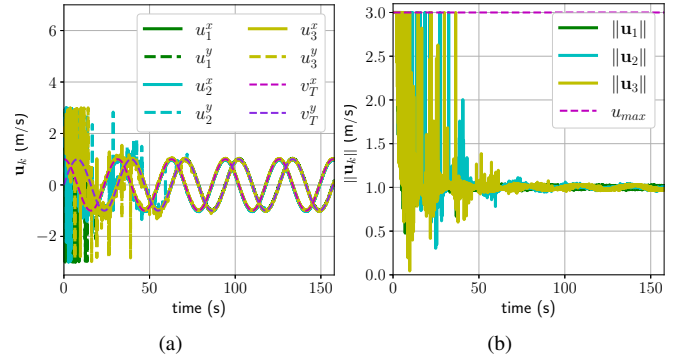


Fig. 7. Control inputs for circular motion of target. (a) BLF-control components tracking target velocity  $\mathbf{v}_T = [\cos 0.2t, \sin 0.2t]$  m/s and (b) control magnitudes satisfying the bound  $u_{\max} = 3$  m/s

its associated standoff circle are plotted in dashed and solid magenta lines, respectively. The BLF-control ensures that the formation is pseudo-rigid and is capable of translating, rotating and deforming, but not rearranging (cyclic order of the agents is unaffected). The agents may rearrange their cyclic order in the formation under QLF-control. Agent 2 moves across the line joining Agents 1 and 3 - the formation transitions through the condition  $d_{1,2} + d_{2,3} = d_{3,1}$ , seen in Fig. 4(b).

The individual components of BLF-control and magnitudes for the agents are plotted in Fig. 5. The agent velocities (control inputs) asymptotically converge to the target velocity (see Fig. 5(a)). The control inputs also satisfy the  $u_{\max}$  bound placed on them as seen in Fig. 5(b).

2) *Circular motion of the target.* The target moves on a circle of radius  $R_T = 5$  m with a speed of 1 m/s. We consider Gaussian noise with standard deviation of 0.02 m/s in an agent's estimates of the target velocity components. The distance measurements are assumed to have noise with standard deviation of 0.02 m.

As in the case of straight-line motion of the target, the BLF-control restricts the deviation from the desired inter-agent distances within the specified bounds despite the noise in the target velocity and distance measurements (see Fig. 6(a)). Thus the formation of agents does not rearrange its cyclic order as seen in Fig. 6(c), where the agents settle on the standoff circle about the target executing circular motion. The standoff circle and the circular trajectory of the target are marked by solid and dashed magenta lines, respectively. The 3 agents move on separate circles, with radii being equal to  $R_T$  but having different centres (Fig. 6(c)). Similarly, the QLF-control makes the 3 agents move on separate circles, however, with a changed cyclic order of the agents compared to the initial order (see Fig. 6(d)). This reordering happens in the initial few seconds of the simulation, as is seen in Fig. 6(b) where the formation transitions through the condition  $d_{1,2} + d_{2,3} = d_{3,1}$  as in the case of straight-line motion of the target.

The control bound  $u_{\max}$  is satisfied as seen in Fig. 7(b). The control inputs to the agents display chatter due to noise in the measurements and operation of the system close to

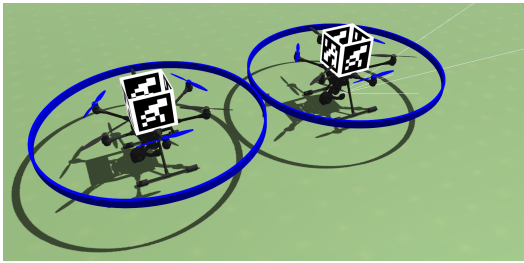


Fig. 8. Gazebo environment with Typhoon multi-rotors

the specified distance bounds (see Figs. 7(a) and 7(b)). The chatter in the control can be correlated to the chatter seen in the inter-agent distances at the beginning of the simulation (in Fig. 6(a)). The control (and inter-agent distance) chatter eventually subside as the inter-agent distances settle to their reference values and the agent velocities match the target velocity in Fig. 7(a). The chatter can be avoided by filtering the distance measurements for the implementation of the algorithm on the UAVs. Another important aspect of designing the algorithm is suitably choosing the distance bounds, accounting for the noise in the velocity and distance measurements. A useful metric for such an analysis may be  $\gamma = \min_{i,j} \min(r_{i,j} - \underline{r}_{i,j}, \bar{r}_{i,j} - r_{i,j}) / SD_N$ , where  $SD_N$  is the standard deviation of the noise in the inter-agent distance measurements. In our simulation  $\gamma = 0.14/0.02 = 7$ . A higher value of  $\gamma$  is beneficial in increasing the robustness of the algorithm to noise.

#### IV. ROS ENVIRONMENT SIMULATION RESULTS

We now discuss the implementation of BLF-control to a pair of hexarotors in the ROS simulation environment and discuss its practical applicability.

##### A. Simulation Environment

The control (7) is tested on the Robot Operating System (ROS) using the Gazebo simulator with PX4 Software in the Loop (SITL) simulation. MAVROS is used to communicate with the models via ROS. The SITL mode provides greater flexibility for testing various control algorithms in simulation before implementation on physical UAV models. A pair of Yuneec ‘Typhoon H480’ hexa-rotors are used with each model mounted with four fiducial ArUco marker trackers on top of the hexa-rotors and visible from all four sides. Each model has a 2D lidar from the ROS rplidar package, and an RGB camera mounted on a gimbal. The lidar has a 360° field of view, a maximum range of 8 m and a 5.5 Hz rotation frequency. The camera has 80° field of view and can be set to full 360° yaw using the gimbal. A custom Gazebo world is created to launch the two hexa-rotors and a target. Fig. 8 shows the Gazebo world with the initial positions of the hexa-rotors. The simulation is run at a rate of 60.0 Hz.

##### B. Implementation

The hexa-rotors are initialised at (0, 0, 0) m and (1, 0, 0) m, with an initial mutual distance of 1.0 m in the local coordinate system. We consider three cases:

- 1) stationary target positioned at (5, 5, 4) m
- 2) target moving in a straight line with constant velocity
- 3) target moving in a circle with constant radius

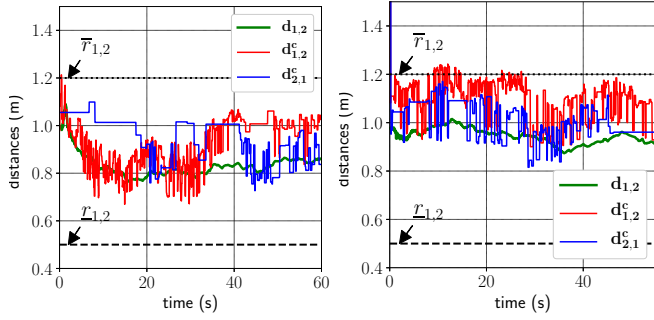
The hexa-rotors take-off and hover at the specified altitude of  $h = 4$  m. The target’s location and velocity are available to the control algorithm of the two hexa-rotors. The lidar data of each hexa-rotor provides the relative angular position of the other one. The camera of each hexa-rotor  $k$  is then yawed to track the position of the other hexa-rotor,  $j$ , using the mounted marker. Using OpenCV image processing library, the marker’s translation and rotation vectors are determined. Appropriate coordinate transformations (10) are performed to determine the position and distance of hexa-rotor  $j$  relative to  $k$  in the local frame of reference  $\mathcal{U}$ , using the camera on hexa-rotor  $k$ ,  $d_{k,j}^c = \|\mathcal{U}\mathbf{x}_{k,j}\|$ ,  $k \in \{1, 2\}$ .

$$\mathcal{U}\mathbf{x}_{k,j} = \mathop{\mathbf{T}}_b^{\mathcal{U}} \mathop{\mathbf{T}}_f^b \mathop{\mathbf{T}}_C^f \mathbf{C}\mathbf{x}_{k,j} \quad (10)$$

where,  $\mathop{\mathbf{T}}_b^{\mathcal{U}}$ ,  $\mathop{\mathbf{T}}_f^b$ , and  $\mathop{\mathbf{T}}_C^f$  are the transformation matrices to transform distance from the hexa-rotor’s body frame to local frame, fixed gimbal frame to the body frame and fixed gimbal frame to the camera’s frame of reference, respectively. The position of Hexa-rotor  $j$  in the frame of reference of the camera on  $k$ , is  $\mathbf{C}\mathbf{x}_{k,j}$ , which is input to the algorithm. Each experiment has desired target standoff circles of  $R_k \in (0.9, 2.0)$  for  $k \in \{1, 2\}$ , and the bounds on inter-hexa-rotor distance as  $\bar{r}_{1,2} \in (1.0, 4.0)$  and  $\underline{r}_{1,2} \in (0.2, 1.0)$  and  $r_{1,2} = \frac{\underline{r}_{1,2} + \bar{r}_{1,2}}{2}$ . The control generated by (7) is input to the hexa-rotors as a reference velocity which the PX4 PID-velocity controller tracks [20].

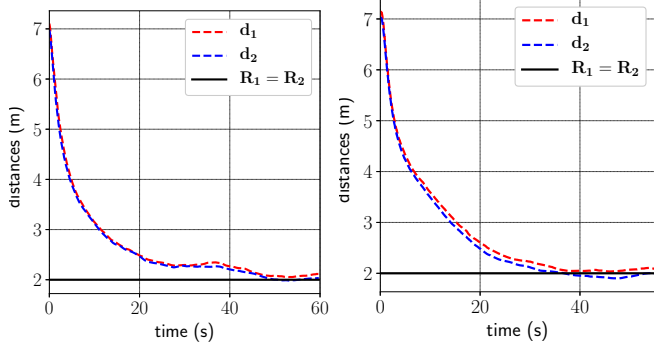
##### C. Experiments and Results

We present a few results with the initial conditions specified above as we vary the inter-hexa-rotor distance bounds starting with  $(\underline{r}_{1,2}, \bar{r}_{1,2}) = (0.2, 2.0)$  and gains  $K = 0.004$ ,  $K_T = 0.02$ . The outer bound is decreased in steps of 0.1 m till 1.3 m. For further decrease in the higher bound,  $K$  is decreased to 0.002 to ensure that the hexa-rotors stay within the bounds. For any further increase in the lower bound, it is required to reduce  $K_T$  to 0.004. A few results of varying the bounds are summarised in Table I. We observe that tighter distance bounds (see Case 3, Table I) lead to higher control inputs to the hexa-rotors due to the barrier function, eventually leading to the transgression of these bounds and oscillatory behaviour. It is thus required to tune the gains  $K_T$  and  $K$  accordingly, which may lead to a slower response (see Case 4, Table I). The results from Case 4 are presented in Fig. 9 along with results of applying QLF-control to the same problem. It is observed that the BLF-control maintains the inter-hexa-rotor distance within bounds and also leads to a faster convergence to the desired inter-hexa-rotor distance of  $r_{1,2} = 0.85$  m, as compared to QLF-control (see Figs. 9(a) and 9(b)) for the same gain values. The low gain values required for keeping the inter-hexa-rotor distance bounded adversely affect the hexa-rotor-target distance tracking. However, this problem may be addressed with gain-scheduling.



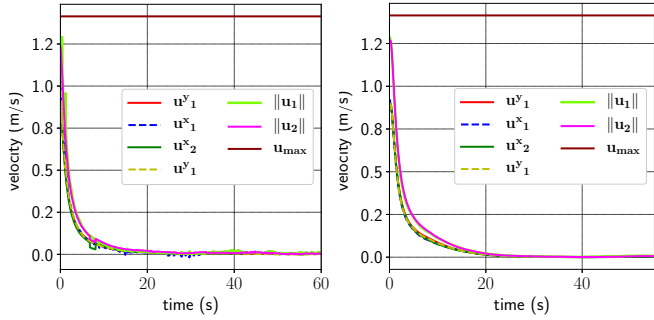
(a) BLF: Inter-hex distance

(b) QLF: Inter-hex distance



(c) BLF: Target-hex distance

(d) QLF: Target-hex distance



(e) BLF: Control Inputs

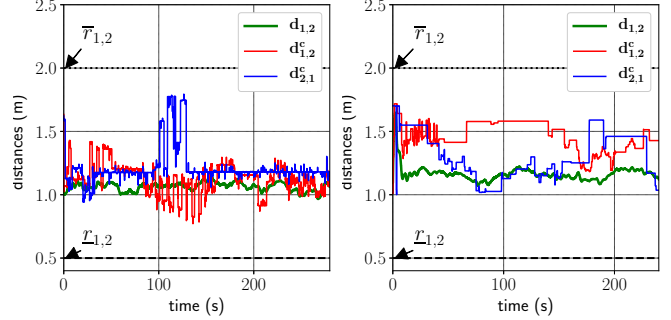
(f) QLF: Control Inputs

Fig. 9. BLF and QLF Control: Control inputs (velocities), inter-hexa-rotor and target-hexa-rotor distances

TABLE I

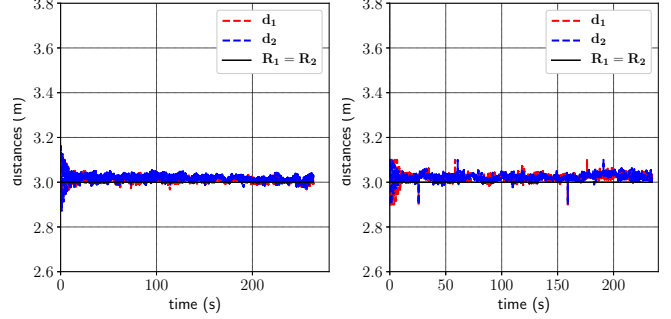
SUMMARY OF RESULTS FOR INTER-HEXA-ROTOR BOUNDS AND GAIN VARIATION,  $R_1 = R_2 = 2$  M FOR A STATIONARY TARGET

S.no.	Hex-Target	Inter-Hex			Observations
	$K_T$	$\underline{r}_{i,j}$	$\bar{r}_{i,j}$	$K$	
1	0.02	0.5	2.0	0.004	Inter-hexa-rotor distance stays within bounds, fast convergence to desired distances
2	0.02	0.5	1.3	0.004	
3	0.02	0.5	1.2	0.004	System does not stay within bounds, does not converge to the desired distances
4	0.004	0.5	1.2	0.002	Inter-hexa-rotor distance stays within bounds, converges to the desired distances slowly due to the reduced gains



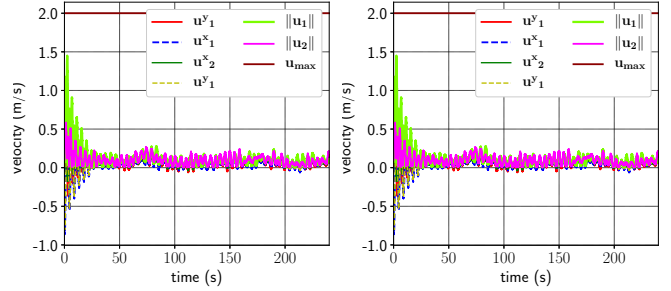
(a) Circular: Inter-hex distance

(b) Straight: Inter-hex distance



(c) Circular: Target-hex distance

(d) Straight: Target-hex distance



(e) Circular: Control Inputs

(f) Straight: Control Inputs

Fig. 10. BLF Control on Circular and Straight trajectories: Control inputs (velocities), inter-hexa-rotor and target-hexa-rotor distances

We extend the tests from a stationary target to a target moving with constant velocity and a target moving along a circular trajectory. We vary the inter-hexa-rotor distance bounds starting with  $(r_{1,2}, \bar{r}_{1,2}) = (0.5, 2.0)$  m and gains  $K = 0.0075, K_T = 0.015$ . The target is given a speed of 0.11 m/s along the straight line  $y = x$ . For the circular target motion, the target moves with a speed of 0.17 m/s and tracks a circle of radius of 10 m with centre at the origin of the simulator. The hexa-rotors are required to maintain a distance of 3.0 m from the target. We summarise the results for the case of straight-line and circular motion of the target in Table II and Table III, respectively. We observe the hexa-rotors are able to strictly maintain the desired hexa-rotor-target distances along with the inter-hexa-rotor distance when the target is moving at this velocity (see Case 1, Tables II, III). When we decrease the outer bound to 1.3 m, we reduce the gains  $K$  and  $K_T$  to lower values to ensure hexa-rotors maintain desired distances (see Case 2, Tables II, III). At higher target velocities, the

TABLE II

SUMMARY OF RESULTS FOR INTER-HEXA-ROTOR BOUNDS AND GAIN VARIATION,  $R_1 = R_2 = 3$  M, FOR A TARGET MOVING IN A STRAIGHT LINE

Case	$v_T$	Inter-Hex			Hex-Target	Observations
	m/s	$\underline{r}_{i,j}$	$\bar{r}_{i,j}$	$K$	$K_T$	
1	0.11	0.5	2.0	0.0075	0.015	Inter-hexa-rotor distance stays within bounds, fast convergence to desired distances
2	0.11	0.5	1.3	0.005	0.001	Inter-hexa-rotor distance stays within bounds, very slow convergence to desired distances
3	0.17	0.5	2.0	0.045	0.0175	System exhibits oscillatory behaviour about the desired target-hex position, while maintaining inter-hex distances
4	0.17	0.5	1.3	0.001	0.0012	System exhibits oscillatory behaviour about the desired target-hex position, very slow convergence to desired distances

TABLE III

SUMMARY OF RESULTS FOR INTER-HEXA-ROTOR BOUNDS AND GAIN VARIATION,  $R_1 = R_2 = 3$  M, FOR A CIRCULARLY MOVING TARGET

Case	$v_T$	Inter-Hex			Hex-Target	Observations
	m/s	$\underline{r}_{i,j}$	$\bar{r}_{i,j}$	$K$	$K_T$	
1	0.17	0.5	2.0	0.015	0.015	Inter-hexa-rotor distance stays within bounds, fast convergence to desired distances
2	0.17	0.5	1.3	0.0036	0.015	Inter-hexa-rotor distance stays within bounds, slow convergence to desired distances
3	0.6	0.5	2.0	0.045	0.0125	System exhibits oscillatory behaviour about the desired target-hex position, while maintaining inter-hex distances
4	0.6	0.5	1.3	0.0036	0.0125	System exhibits oscillatory behaviour about the desired target-hex position, slow convergence to inter-hex distances

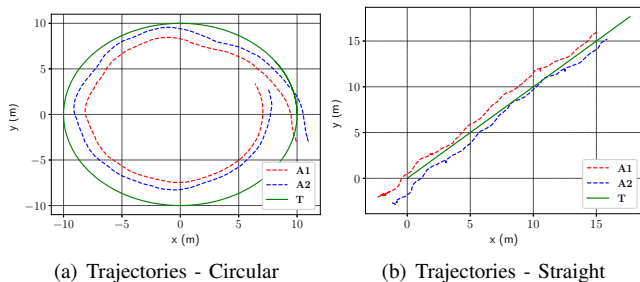


Fig. 11. Target-Agent trajectories; T - target; A1, A2 - agents

gains  $K$  and  $K_T$  are increased to enable the hexa-rotors to quickly reach the target, leading to a fast response from the hexa-rotors and oscillatory behaviour about the desired hexa-rotor-target distance (see Case 3, Table II). For the circular motion of the target, we tune the gains by increasing  $K$  and decreasing  $K_T$  such that the hexa-rotors can track the target while maintaining the desired separation (see Case 3, Table III). For a smaller inter-hexa-rotor bound, the gain  $K$  is significantly reduced to ensure the hexa-rotors maintain the desired bounds (see Case 4, Tables II, III). The results of BLF-control for Case 1 and for straight and circular motion of the target are presented in Figs. 10 and 11.

The simulation results are presented with camera-based sensing of distance, and pitching of the hexa-rotors (and the camera, lidar) affects the accurate sensing of this distance. This makes it difficult to precisely track the other hexa-rotor

and maintain the inter-hexa-rotor distance within bounds. We expect accurate sensing and inter-agent communication of positions/distances with a 3D lidar system to improve the performance of the proposed BLF-control.

#### D. Application and Extension of the Problem

The ROS implementation results of control (7) applied to a two-hexa-rotor target tracking application can be extended to a problem with multiple hexa-rotors. Such a target tracking application would require a *ring* topology for the agents to surround the target. Further, assuming a virtual agent ( $A_v$ ) to be located at the centroid of this formation, the entire formation can be made to track a physical target (T) by making  $A_v$  track T (see Fig. 12). Additionally, by changing the function  $U(\mathbf{x}, \mathbf{x}_{A_v})$  (3) to a BLF, the *ring* formation with the virtual agent will be preserved (assuming the virtual agent's velocity information is available to the surrounding agents).

The work presented in this paper is also applicable to formation preservation in the presence of obstacles. The obstacle avoidance objective may be accounted for as a repulsion component in an agent's multi-objective control, and the BLF component of control will allow the formation to deform minimally in the vicinity of obstacles. However, the augmented control requires an analysis of the undesired equilibria of the system introduced by the addition of the obstacle avoidance component.



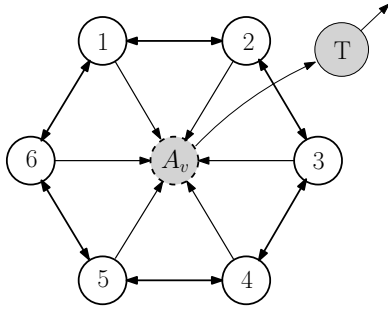


Fig. 12. A system of  $N = 6$  agents tracking a virtual agent with distance bounds, as the virtual agent tracks a target. Directional arrows indicate tracking of an agent; bi-directional arrows indicate mutual tracking of agents

## V. CONCLUSIONS AND FUTURE WORK

Formation preservation is an important requirement of many proposed multi-agent surveying and tracking applications. We presented a BLF-based control law to preserve the inter-agent distances in a formation as applied to a collaborative target tracking application. The Lyapunov stability of the proposed control law was proved, and the formulation of a formation as a collection of bounded inter-agent distances was presented. This formulation can be easily extended to physical multi-robot formations.

The extensive ROS environment simulations presented for a pair of hexa-rotors tracking targets executing constant velocity and circular motion provided valuable insights about the implementation of the algorithm in real-world applications, the shortcomings and possible solutions to address them. The extension of the algorithm to applications with multiple hexa-rotors and obstacle avoidance was also discussed and is in scope for future work. A further analysis on the effects of control input saturation, quantifiable guarantees on steady-state errors, and undesired equilibria is also planned. Associated ROS environment simulations and eventual implementation of the algorithms on a team of multi-rotors will help in further evaluation of the advantages of the control proposed in this paper.

## REFERENCES

- [1] H. Li, A. V. Savkin, and B. Vucetic, "Autonomous area exploration and mapping in underground mine environments by unmanned aerial vehicles," *Robotica*, vol. 38, no. 3, p. 442–456, 2020.
- [2] M. Kulbacki, J. Segen, W. Knieć, R. Klempous, K. Kluwak, J. Nikodem, J. Kulbacka, and A. Serester, "Survey of drones for agriculture automation from planting to harvest," in *22nd IEEE International Conference on Intelligent Engineering Systems (INES)*, 2018, pp. 353–358.
- [3] F. Arab, F. A. Shirazi, and M. R. Hairi Yazdi, "Cooperative parameter estimation of a nonuniform payload by multiple quadrotors," *Robotica*, pp. 1–20, 2021.
- [4] Y. Altshuler, V. Yanovsky, I. A. Wagner, and A. M. Bruckstein, "Efficient cooperative search of smart targets using uav swarms," *Robotica*, vol. 26, no. 4, pp. 551–557, 2008.
- [5] S. Li and D.-Y. Yeung, "Visual object tracking for unmanned aerial vehicles: A benchmark and new motion models," *Proceedings of the AAAI Conference on Artificial Intelligence*, vol. 31, no. 1, Feb. 2017.
- [6] J. Li, D. H. Ye, T. Chung, M. Kolsch, J. Wachs, and C. Bouman, "Multi-target detection and tracking from a single camera in unmanned aerial vehicles (UAVs)," in *IEEE/RSJ International Conference on Intelligent Robots and Systems (IROS)*, 2016, pp. 4992–4997.

- [7] M. Mueller, G. Sharma, N. Smith, and B. Ghanem, "Persistent aerial tracking system for UAVs," in *IEEE/RSJ International Conference on Intelligent Robots and Systems (IROS)*, 2016, pp. 1562–1569.
- [8] E. Schwalb and J. Schwalb, "Improving redundancy and safety of UTM by leveraging multiple uass," in *International Conference on Unmanned Aircraft Systems (ICUAS)*, 2019, pp. 100–110.
- [9] J. Han and Y. Chen, "Cooperative source seeking and contour mapping of a diffusive signal field by formations of multiple uavs," in *International Conference on Unmanned Aircraft Systems (ICUAS)*, 2013, pp. 35–40.
- [10] L. Moreau, "Stability of multiagent systems with time-dependent communication links," *IEEE Transactions on Automatic Control*, vol. 50, no. 2, pp. 169–182, 2005.
- [11] L. Sabattini, C. Secchi, and N. Chopra, "Decentralized estimation and control for preserving the strong connectivity of directed graphs," *IEEE Transactions on Cybernetics*, vol. 45, no. 10, pp. 2273–2286, 2015.
- [12] M. Egerstedt and Xiaoming Hu, "Formation constrained multi-agent control," *IEEE Transactions on Robotics and Automation*, vol. 17, no. 6, pp. 947–951, 2001.
- [13] D. Panagou, D. M. Stipanović, and P. G. Voulgaris, "Distributed coordination control for multi-robot networks using Lyapunov-like barrier functions," *IEEE Transactions on Automatic Control*, vol. 61, no. 3, pp. 617–632, 2016.
- [14] D. Han and D. Panagou, "Robust multitask formation control via parametric Lyapunov-like barrier functions," *IEEE Transactions on Automatic Control*, vol. 64, no. 11, pp. 4439–4453, 2019.
- [15] S. Zhao and D. Zelazo, "Bearing rigidity theory and its applications for control and estimation of network systems: Life beyond distance rigidity," *IEEE Control Systems Magazine*, vol. 39, no. 2, pp. 66–83, 2019.
- [16] K. P. Tee, S. S. Ge, and E. H. Tay, "Barrier Lyapunov functions for the control of output-constrained nonlinear systems," *Automatica*, vol. 45, no. 4, pp. 918–927, 2009.
- [17] S. Gul, E. Zergeroglu, E. Tatlicioglu, and M. V. Kilinc, "Desired model compensation-based position constrained control of robotic manipulators," *Robotica*, pp. 1–15, 2021.
- [18] A. Keymasi Khalaji and R. Zahedifar, "Lyapunov-based formation control of underwater robots," *Robotica*, vol. 38, no. 6, pp. 1105–1122, 2020.
- [19] M. Khaledyan and M. de Queiroz, "A formation maneuvering controller for multiple non-holonomic robotic vehicles," *Robotica*, vol. 37, no. 1, pp. 189–211, 2019.
- [20] L. Meier, D. Honegger, and M. Pollefeys, "PX4: A node-based multithreaded open source robotics framework for deeply embedded platforms," in *IEEE International Conference on Robotics and Automation (ICRA)*, 2015, pp. 6235–6240.
- [21] W. Meng, Z. He, R. Su, A. R. Shehabinia, L. Lin, R. Teo, and L. Xie, "Decentralized control of multi-UAVs for target search, tasking and tracking," *IFAC Proceedings Volumes*, vol. 47, no. 3, pp. 10048–10053, 2014, 19th IFAC World Congress.
- [22] N. Michael, J. Fink, and V. Kumar, "Cooperative manipulation and transportation with aerial robots," *Autonomous Robots - AROBOTS*, vol. 30, pp. 73–86, 2011.
- [23] A. Jain and D. Ghose, "Trajectory-constrained collective circular motion with different phase arrangements," *IEEE Transactions on Automatic Control*, vol. 65, no. 5, pp. 2237–2244, 2020.